

IMPROVING THE COMPRESSIVE PERFORMANCE OF ADVANCED GRID STRUCTURES

M.J. Donough¹, C. Zhao², and B.G. Prusty^{1*}

¹ ARC Training Centre for Automated Manufacture of Advanced Composites, University of New South Wales, Sydney, Australia

² College of Mechanical & Electrical Engineering, Nanjing University of Aeronautics & Astronautics, Nanjing, PR China

* Corresponding author (g.prusty@unsw.edu.au)

Keywords: *Advanced grid structures, Automated fiber placement, Mechanical testing*

ABSTRACT

Optimized advanced grid structures can realize significant weight savings than conventional stringer stiffened structures. The overlapping of the transverse grid stiffeners can induce tow waviness at the intersection region whereas localized buckling at the intersection regions is evident under compressive loading. Automated fiber placement-based manufacturing method is proposed here to improve the compressive performance of the grid stiffeners by using the clamp-cut-restart method. Tows are laid until the lateral and transverse grid's intersection and then cut. The tow laying is then restarted after the grid intersection. Therefore, cut-tows are introduced into grid stiffeners to remove excessive material at the intersection. The influences of tow waviness and cut-tows on the microstructure, mechanical performance of grid stiffener is investigated using experimental and finite element methods. Results show that structural efficiency of grid stiffener can be improved significantly with appropriate ratio of cut-tows at the intersection of grid stiffener. Corresponding finite element models are developed for verification and established good correlation with the experimental response. The finite element analyses also provide an insight on the distribution effects of the cut tows. The results of this study can be further used towards the design and manufacture of advanced grid structures for improved compressive performance.

1 INTRODUCTION

Advanced grid structures (AGS) are highly optimized structures where the distribution and orientation of the grids are optimized to provide structural stability under compression. As a result, the weight savings are more significant compared to traditional stringer-stiffened design [1, 2], and this is especially advantageous for aerospace applications. Typical grid-stiffened configurations include orthogrid, isogrid, and Kagome.

The typical fabrication process of AGS is performed by laying continuous carbon fiber tows into a silicone mold via filament winding [3]. During the autoclave curing process, the mold expands and provides lateral compaction to the grid stiffeners. However, as continuous tows are laid across the grid intersections, this creates excess material, thickness and tow waviness at this region [4]. Under compressive loads, the tow waviness will lead to secondary bending and micro buckling of fibers [5, 6]. Consequently, this leads to a reduction in mechanical performance. The authors [4] reported earlier that the failure location of AGS occurs at the grid intersections. Micromechanics modelling and prediction requires heavy computational effort and is not feasible for large structures. During the design and optimization process, efficient analytical methods such as smeared stiffeners method [7], arbitrarily oriented stiffener formulation [8], and asymptotic homogenization method [9] are used. Conservative safety factors are employed to account for the knockdown in performance in these regions, negating some of the weight saving benefits. Zhao et al. [4] performed a detailed finite element modelling of the grid stiffener's intersection under flexural loads. Subsequently, taking inspiration from biological

composites [10], a parametric modelling study was performed to investigate the enabling mechanisms to induce a gradual fracture of thick AGS grid stiffeners [11]. Rodriguez-Garcia and Guzman de Villoria [12] also implemented a cut-tow design method in composite laminates using automated fiber placement to generate a gradual fracture under tensile loads.

The current work presents a cut-tow design of the grid stiffener intersections to reduce the excess material and tow waviness to improve compressive strength. The cut-tow design was manufactured using automated fiber placement (AFP) using the clamp-cut-restart method. Compressive testing of a coupon level representation of the AGS was conducted to investigate if the cut-tow designs were able to improve the compressive strength of the grid stiffener intersections. A detailed characterization and modelling of the AGS was also performed. If the trials were successful, a lower safety factor can be used to maximize the weight saving benefits of an AGS.

2 EXPERIMENT METHODOLOGY

2.1 Manufacturing

The material used for AFP is a unidirectional carbon fiber/epoxy towpreg, with a fiber volume fraction of 63% and a nominal thickness of 0.15 mm. The width of the towpreg is 10 mm. The grid stiffeners were first laid by AFP into a mold with a compaction force of 500 N, layup speed of 200 mm/min and a nip point temperature of 30 °C.

The cut-tows designs were implemented at the grids' intersection using the clamp-cut-restart procedure of AFP, as illustrated in Fig. 1. During the towpreg placement on the longitudinal grids, the placement head will clamp and cut the incoming towpreg as it approaches the grid intersection. The remaining towpreg length is laid on the longitudinal grids and no material is placed in the intersection region, seen in Fig.1, after the placement head moves across the intersection, placement in the longitudinal grids is then restarted. This allows continuous towpreg to be laid in the transverse grids without creating excessive tow waviness. This was also performed for the transverse grids to investigate the distribution and the effects of microstructure on the compressive strength. The grid stiffeners were vacuum bagged and cured in an autoclave for 180 °C for 120 minutes and a pressure of 6 bar. The transverse grids were then machined off and cut into dimensions of 10mm (width) × 150 mm (length).

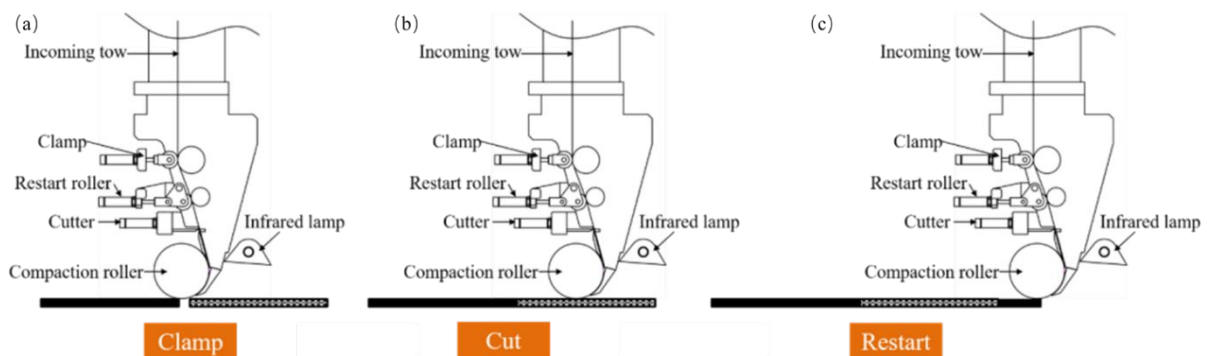


Fig. 1 The placement head (a) clamps and (b) cuts the incoming tow as it reaches the grid intersection. No material is laid at the intersection. Then, (c) layup is restarted after the placement head passes the intersection.

For the thin specimens, there were a total of eight plies in the transverse and longitudinal grids. Two configurations were manufactured: one with continuous overlaps and the other with cut-tows at the intersection. The naming convention of the specimen, *SG-m-nbyn*, are as follows: *SG* is for straight grid, *m* denotes the ratio of cut tows, *n* denotes the number of repetitive tows of the same orientation. Fig. 2 schematically shows the stacking sequence and distribution of the cut-tows at the grid intersection. The thick specimens consist of 20 plies in the longitudinal and transverse grids. The naming convention

of the thick specimen is the same with the exception of the id **SGT** to represent that this is for straight grid thick. The rib thickness (T_r) of SG and SGT are 1.2 mm and 3 mm, respectively. The design configurations of the thin and thick specimens are summarized in Table 1.

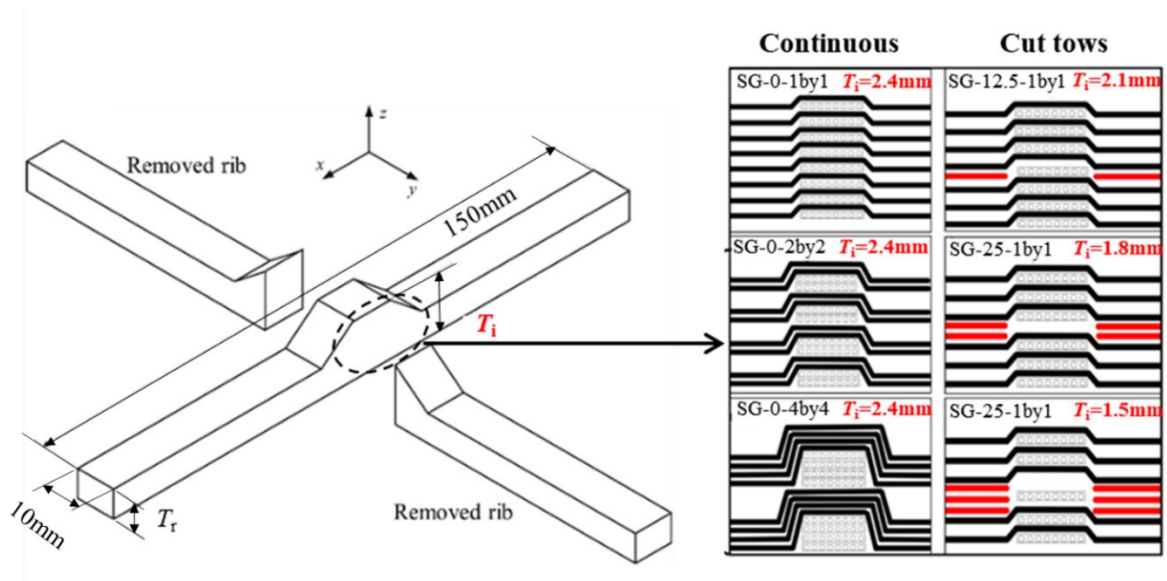


Fig. 2 Specimen manufacturing configuration.

Table 1. Grid intersection design configuration.

Specimen ID	Category	% cut-tows	Stacking sequence at intersection
SG-0-1by1	Thin	0	$[90/0]_8$
SG-0-2by2	Thin	0	$[90/90/0/0]_4$
SG-0-4by4	Thin	0	$[90/90/90/90/0/0/0/0]_2$
SG-12.5-1by1	Thin	12.5	$[90/0/90/0/90/0/90/0/90/0/90/0/90/0/90/0]_*$
SG-25-1by1	Thin	25	$[90/0/90/0/90/0/90/0/90/0/90/0/90/0/90/0]$
SG-37.5-1by1	Thin	37.5	$[90/0/90/0/90/0/90/0/90/0/90/0/90/0/90/0]$
SGT-0-1by1	Thick	0	$[90/0]_{20}$
SGT-10-1by1	Thick	10	$[90/0/90/0/90/0/90/0/90/0]_4$
SGT-20-1by1	Thick	20	$[90/0/90/0/90/0/90/0/90/0]_4$
SGT-30-1by1	Thick	30	$[90/0/90/0/90/0/90/0/90/0]_4$
SGT-40-1by1	Thick	30	$[90/0/90/0/90/0/90/0/90/0]_4$

* Underlined plies are discontinuous in the intersection of stiffeners.

2.2 Optical microscopy

The tow waviness at the grid intersections was investigated with optical microscope (Leica DVM5000). The ratio of the thickness to half-span of the grids intersection, λ , is given as A/L . The tow waviness angle, θ , was used to describe the degree of tow waviness and characterized as presented in Fig 3.

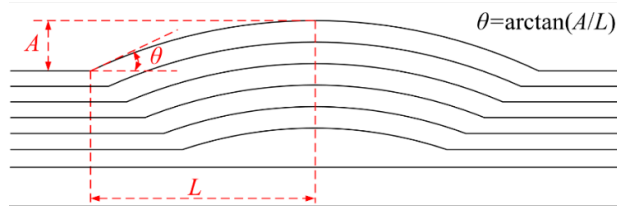


Fig. 3 Microstructure and characterization of tow waviness at the grid intersection.

2.3 Compression tests

The compression tests were carried out in accordance with ASTM D6641 with a controlled cross head displacement of 1.5 mm/min. Tabs of 65 mm in length were adhered on both ends.

3 FINITE ELEMENT MODELLING

A three-dimensional finite element (FE) model was developed using Abaqus 2020 to predict the failure mechanisms of the AGS under compression. The AGS geometry was modelled tow by tow and the tow waviness angle was modelled after the optical microscopy analysis. The curved feature around the intersection was assumed to be flat in order to simplify the modelling process. The composite tows were meshed with continuum shell elements and only the gauge length between the grips was modelled. Between every tow, a traction interface was defined. The schematic of the FE model and boundary conditions is shown in Fig. 4. The traction definition had a quadratic stress delamination initiation criterion as follows:

$$\left\{ \frac{t_n}{t_n^0} \right\}^2 + \left\{ \frac{t_s}{t_s^0} \right\}^2 + \left\{ \frac{t_t}{t_t^0} \right\}^2 = 1 \quad (1)$$

The subscripts, n, s and t , denotes the stresses in the normal (mode I), shear (mode II) and tearing (mode III) directions respectively. The superscript, 0, denotes the maximum traction stresses. Final failure of the interface was given by the fracture energy based criterion:

$$\left\{ \frac{G_n}{G_n^0} \right\}^2 + \left\{ \frac{G_s}{G_s^0} \right\}^2 + \left\{ \frac{G_t}{G_t^0} \right\}^2 = 1 \quad (2)$$

The composite tows were meshed with SC8R continuum shell elements. The intralaminar damage of the composites tows were modelled using Hashin failure criteria [13]. There are four damage modes and are given as:

$$\text{Fiber tension:} \quad F_f^t = \left(\frac{\sigma_{11}}{X^T} \right)^2 + \alpha \left(\frac{\tau_{12}}{SL} \right)^2 \quad (3)$$

$$\text{Fiber compression:} \quad F_f^c = \left(\frac{\sigma_{11}}{X^c} \right)^2 \quad (4)$$

$$\text{Matrix tension:} \quad F_m^t = \left(\frac{\sigma_{11}}{Y^T} \right)^2 + \left(\frac{\tau_{12}}{SL} \right)^2 \quad (5)$$

$$\text{Matrix compression:} \quad F_m^c = \left(\frac{\sigma_{22}}{2S^T} \right)^2 + \left[\left(\frac{Y^c}{2S^T} \right)^2 - 1 \right] \frac{\sigma_{22}}{Y^c} + \left(\frac{\tau_{12}}{SL} \right)^2 \quad (6)$$

X^T and X^C are the ultimate tensile and compressive stress in the longitudinal direction respectively; Y^T and Y^C are the ultimate tensile and compressive stress in the transverse direction respectively; S^L and S^T are the longitudinal and transverse shear failure stress respectively; α is a coefficient that defines the contribution of the shear stress to the fiber tensile initiation criterion, which is taken as one. Table 2 details the material properties of the carbon fiber/epoxy composites.

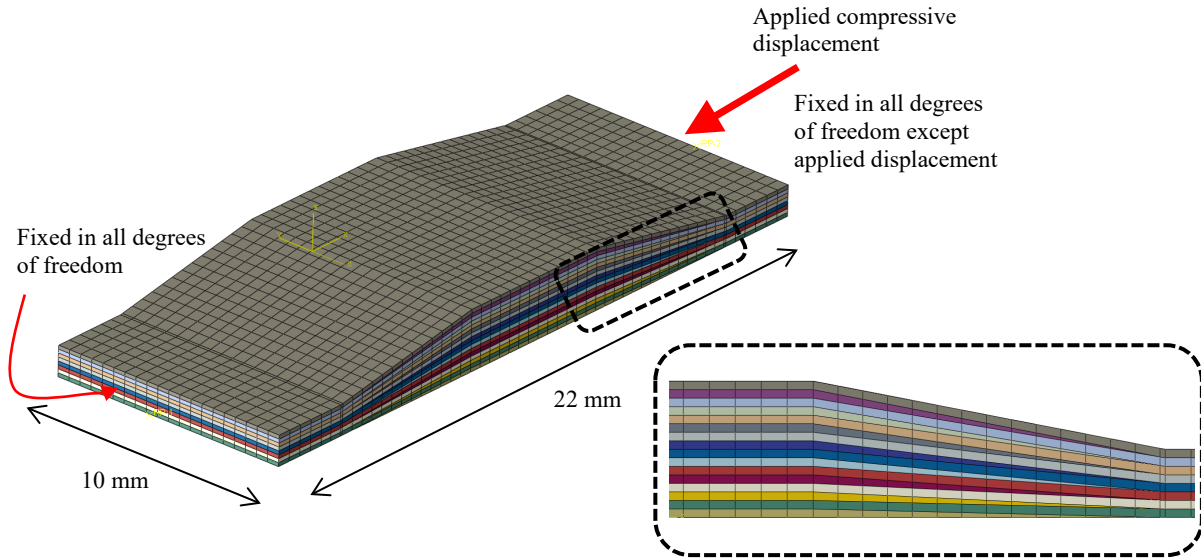


Fig. 4 Finite element boundary and loading conditions.

Table 2. Mechanical properties of EM118/A10 towpreg

Symbol	Description	Value	Unit	Symbol	Description	Value	Unit
E_{11}	Longitudinal modulus	122	GPa	X_T	Longitudinal tensile strength	2156	MPa
E_{22}	Transverse modulus	7.5	GPa	X_C	Longitudinal compressive strength	1157	MPa
E_{33}	Through-thickness modulus	7.5	GPa	Y_T	Transverse tensile strength	36.3	MPa
G_{12}	In-plane shear modulus 12	3.7	GPa	Y_C	Transverse compressive strength	145	MPa
G_{13}	Out-plane shear modulus	3.7	GPa	S_L	Longitudinal shear strength	110	MPa
G_{23}	Out-plane shear modulus	4.0	GPa	S_T	Transverse shear strength	55	MPa
t_n^0	Maximum normal traction stress	68	MPa	t_s^0	Maximum shear traction stress	39.3	MPa
t_t^0	Maximum tearing traction stress	39.3	MPa	G_n^0	Critical normal fracture energy	0.7	kJ/m ²
G_s^0	Critical shear fracture energy	1.6	kJ/m ²	G_t^0	Critical tearing fracture energy	1.6	kJ/m ²

4 RESULTS

4.1 Tow waviness at the grids' intersection

The optical microscopy images of thin grid's intersection are shown in Fig 5. It can be seen the cross section of cut-tow designs, SG-12.5-1by1 and SG-37.5-1by1, had no significant voids or defects after curing. The same observation was also taken for the thick specimens.

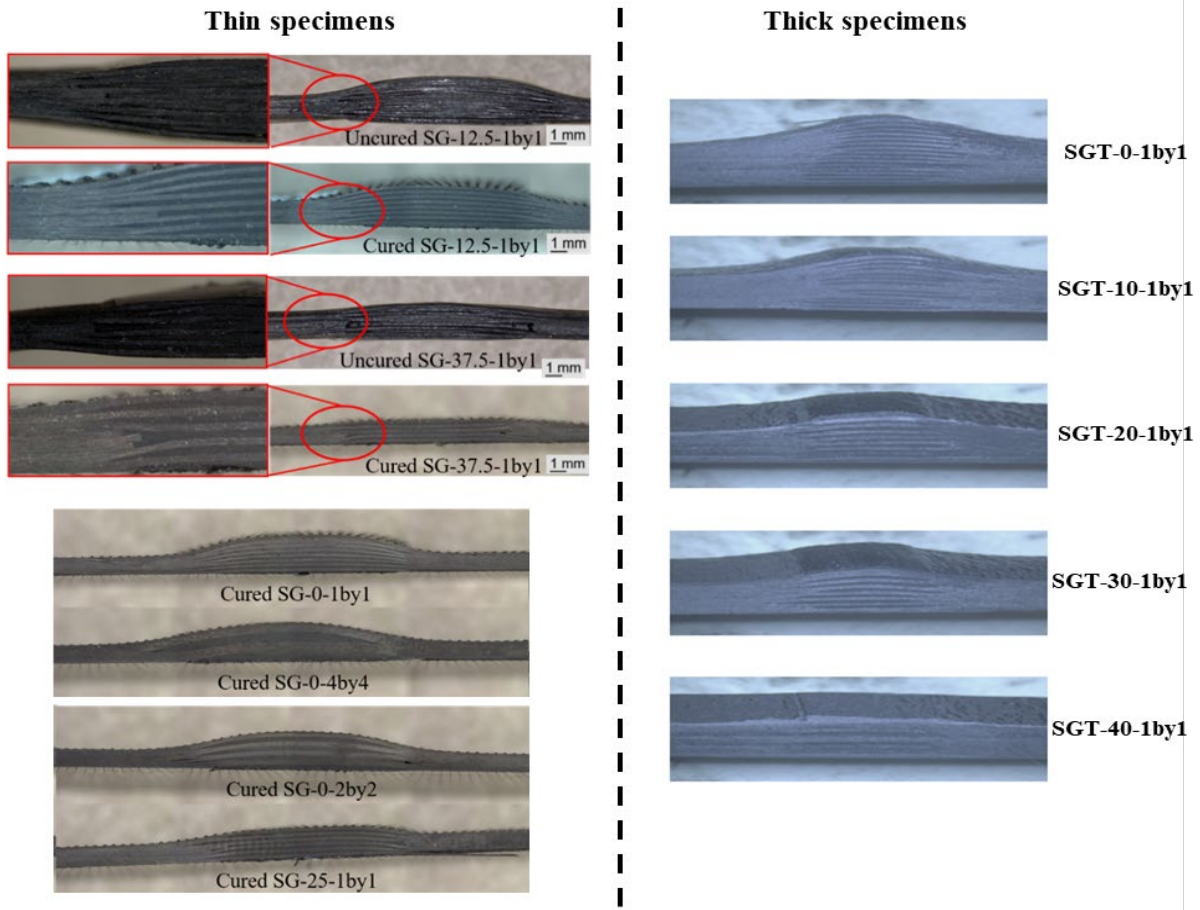


Fig. 5 Tow waviness of thin and thick specimens.

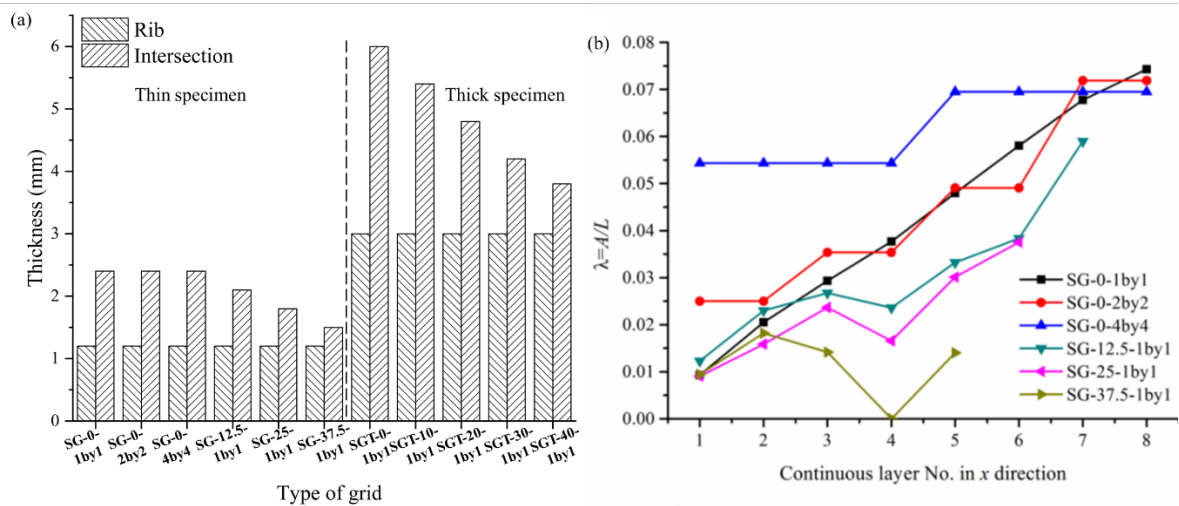


Fig. 6 Grid intersection geometry of the manufactured specimens: (a) thickness difference between rib and intersection and (b) fiber waviness of each ply in thin specimen.

As more cut-tows were used, the difference in the intersection and grid thickness became less pronounced, as presented in Fig. 6(a). The global intersection thickness in SG-0-1by1, SG-0-2by2, and SG-0-4by4 were the same. However, the degree of tow waviness differs in the individual layers, depending of the stacking sequence at the intersection, shown in Fig.6(b). The averaged tow drop-off angle in SG-0-1by1, SG-0-2by2, and SG-0-4by4 were 4.92°, 5.17° and 7.05° respectively. With higher

percentage of cut-tows, the averaged drop-off angle of SG-12.5-1by1, SG-25-1by1 and SG-37.5-1by1 were 6.73 °, 4.29 ° and 1.62 °, much lower than the continuous overlap tow designs. The relation of λ and θ with geometry dimension of grid stiffener for the conventional configuration can be described in an empirical equation and the result of the curve-fitting was defined as:

$$\lambda = 0.0315h + 0.0005 \quad (7)$$

where h is the thickness difference between rib and intersection of grid stiffeners.

4.2 Compressive performance of thin specimens

The experimental and numerical predicted load-displacement curves of the continuous tows designs, SG-0-1by1, SG-0-2by2, and SG-0-4by4, are presented in Fig 7. The onset of non-linearity occurs at varying compressive displacements. This is likely due to the degree of tow waviness at the grid intersection. The tow waviness induced a localized buckling due to load path eccentricity. A larger tow drop-off angle also leads to a reduction in the compressive stiffness and strength of the grid stiffener. The FE model was able to predict the response of the continuous tows grid stiffener's behavior with reasonable accuracy.

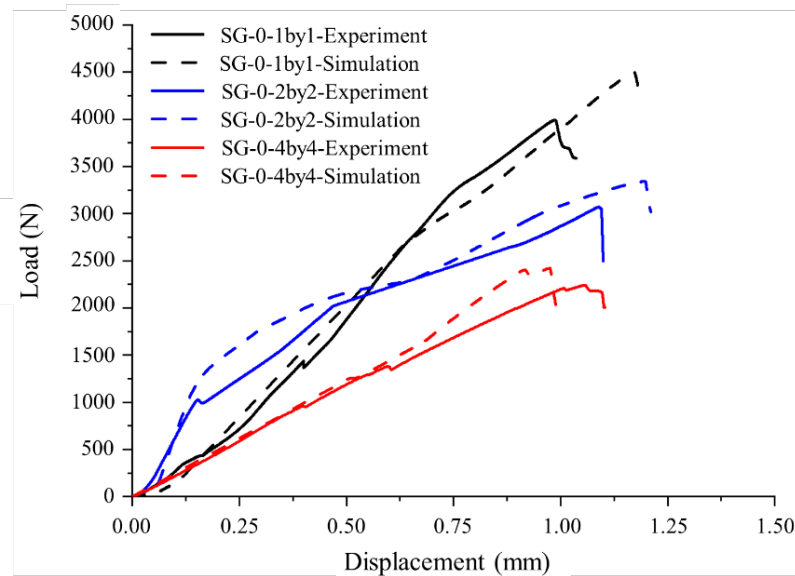


Fig. 7 Experimental and numerical predicted load-displacement response of continuous tows straight grids under compression.

The tow waviness of the cut-tow designs, SG-12.5-1by1, SG-25-1by1, SG-37.5-1by1, were modelled based of the microscopy observations. The FE model predicted the experimental response with good accuracy, as seen in Fig 8. SG-12.5-1by1 had the highest tow drop-off angle in the cut-tow designs which resulted it in having the lowest stiffness. SG-25-1by1 and SG-37.5-1by1 had low tow drop-off angle at the intersection and, hence, the fibers are mostly orientated in the loading direction. Consequently, they had higher stiffness than SG-12.5-1by1. However, SG-12.5-1by1 had the highest compressive strength of the cut-tow designs.

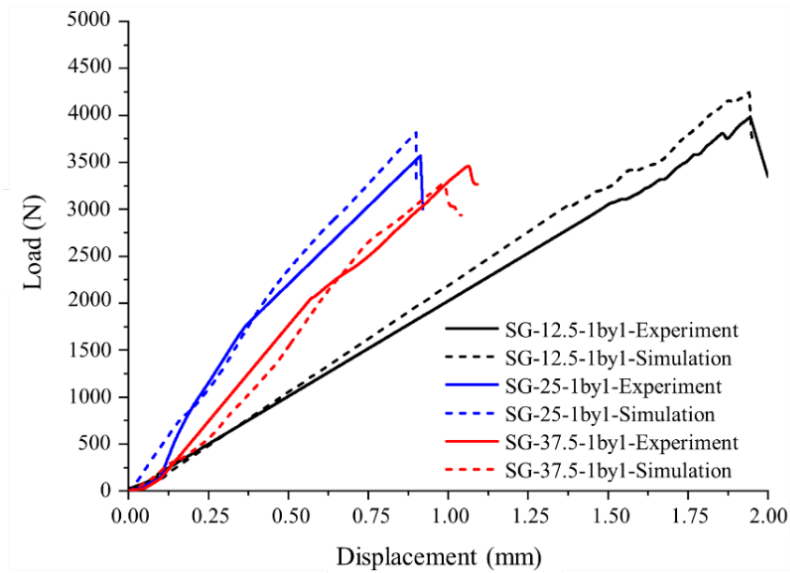


Fig.8 Experimental and numerical predicted load-displacement response of continuous tows straight grids under compression.

The final fracture of the grid stiffeners are shown in Fig. 9. All specimens buckled in a half-sine wave pattern. The FE results showed high stresses at the corner geometry of the intersection where the tows of the lateral grids deviate from the principal loading direction. The individual tows began to kink under increasing compressive loads due to the load eccentricity. This then leads to initiation and propagation of matrix dominated damage and delamination from this location.

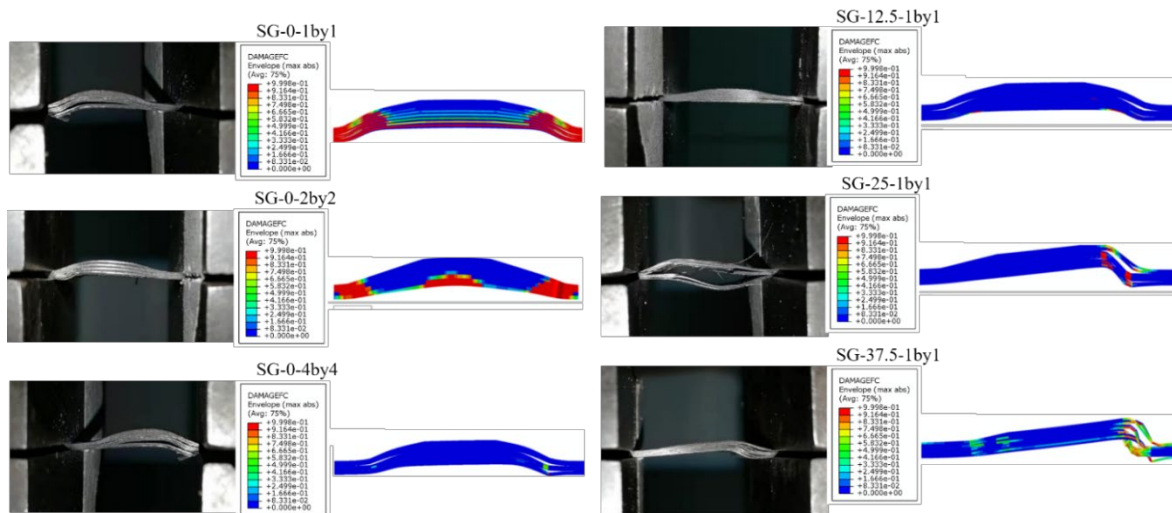


Fig. 9 Final fracture mode of the continuous and cut-tows grid stiffeners.

The compressive strengths of the continuous and cut-tows designs are compared in Fig. 10. The compressive failure load of SG-0-1by1 and SG-0-2by2, and SG-0-4by4 degraded significantly with increasing scale of tow waviness. The compressive strength of SG-0-2by2 and SG-0-1by1 was 70.5% and 52.9% of SG-0-1by1 respectively. Hence it is recommended that the tows of the lateral and transverse grids be alternated at every single layer to reduce the tow drop-off angle. The inclusion of cut-tows led to a reduction in compressive performance of grid stiffeners (SG-12.5-1by1, SG-25-1by1 and SG-37.5-1by1). However, the reduction in ply waviness angle within the cut-tows specimens impeded the tows from kinking prematurely, which can lead to an overall improvement in compressive performance.

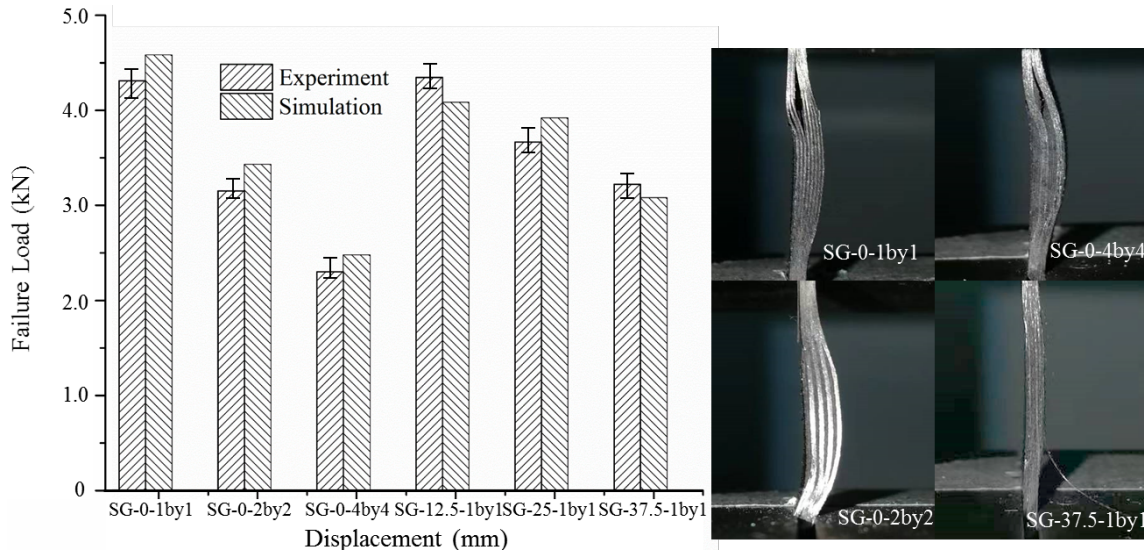


Fig. 10 Compressive failure loads of continuous and cut-tows grid stiffeners.

Based on the experimental and FE studies, the stacking sequence at the grid stiffener intersection affects the compressive performance due to changes in the microstructure. As more tows were distributed on the outer layers, the tow waviness angle increased and, consequently, increased the load path eccentricity. This induced secondary bending moment and localized buckling. The introduction of cut-tows reduces the tow waviness at the grid intersection. Further FE study was carried out to investigate the distribution and location of the cut-tows effect on the compressive strength of SG-0-2by2 configuration. As seen in Fig. 11, the introduction of cut-tows improved the compressive strength of the 2by2 design. This was achieved by reducing the tow drop off angle. Hence, it will be beneficial to have cut-tows if multiple passes in the same orientation or thick tows are used. The location of the cut-tows did not affect the failure mode (which is predominantly by localized buckling) for 25% cut-tows. Moving the cut-tows to the middle or top region for the 37.5% cut-tows improve the failure strength and the failure mode was under compression failure.

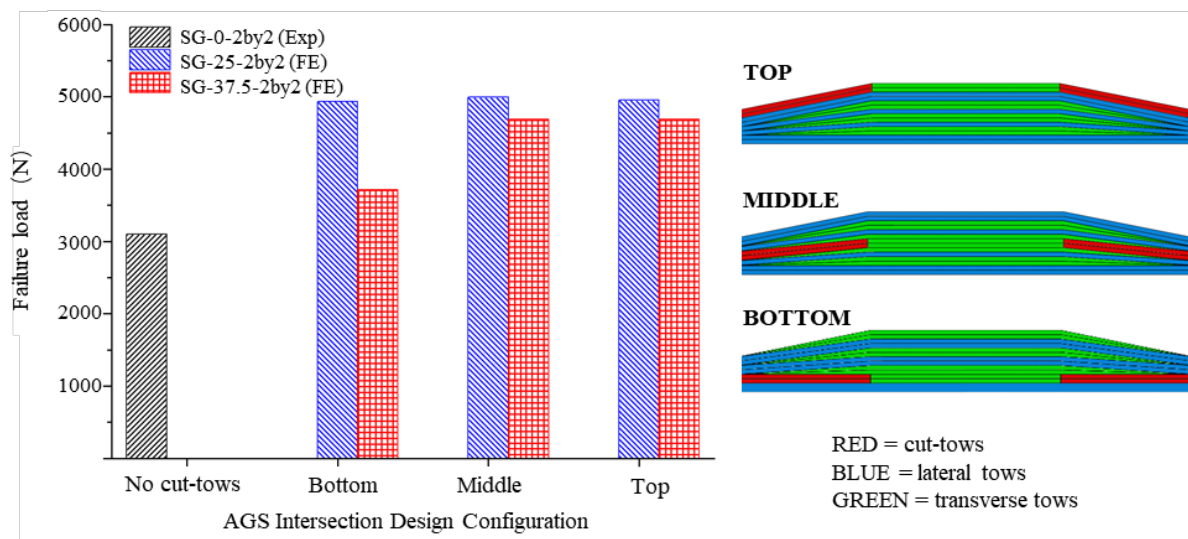


Fig. 11 Compressive failure loads of various cut-tows designs.

4.3 Compressive performance of thick specimens

To verify the scalability of the cut-tows design, compression tests was conducted for the thick grid stiffener with different ratios of cut-tows, as listed in Table 1. In such a representative grid stiffener, the

thickness of rib is 3 mm, which is much larger than the thickness of rib studied above. A tow-drop angle of 14.63° was predicted using Eq. (7) for SGT-0-1by1.

The compressive failure load obtained via experiment for the thick grid stiffener with different cut-tows is presented in Fig. 12. The tow drop-off angle played a significant role in compression performance. Stiffener (SGT-0-1by1), with the highest tow drop-off angle, had the lowest compressive failure load. The introduction of the cut-tows in the intersection did not compromise the bending performance of the grids. The thick grid stiffeners failed catastrophically upon reaching the critical load in a mixture of localized buckling and compressive fiber failure at the kink. The failure mode was similar to the experimental observations. The cut-tows designs showed an improvement in the compressive failure load. This was driven by the reduction in tow drop-off angle and better alignment of the reinforcing fibers with the loading direction. However, SGT-40-1by1 suffered a reduction in compressive failure load compared to SGT-30-1by1. This was because, while the reduction in tow waviness improved the compressive strength, the increase in cut-tows led to a reduction in mechanical stiffness and strength. Hence, the cut-tow design must consider both competing effects and select an appropriate ratio of cut-tows. When the ratio of cut-tows was 30%, these two effects on final performance of grid reached a balance point. Further research on the influence of cut-tows at the intersection of a representative AGS are required to improve confidence and further optimize the design methodology. Further researches on the influence of cut-tows on the compressive strength of thick AGS specimen are needed to improve confidence and further optimize the design methodology.

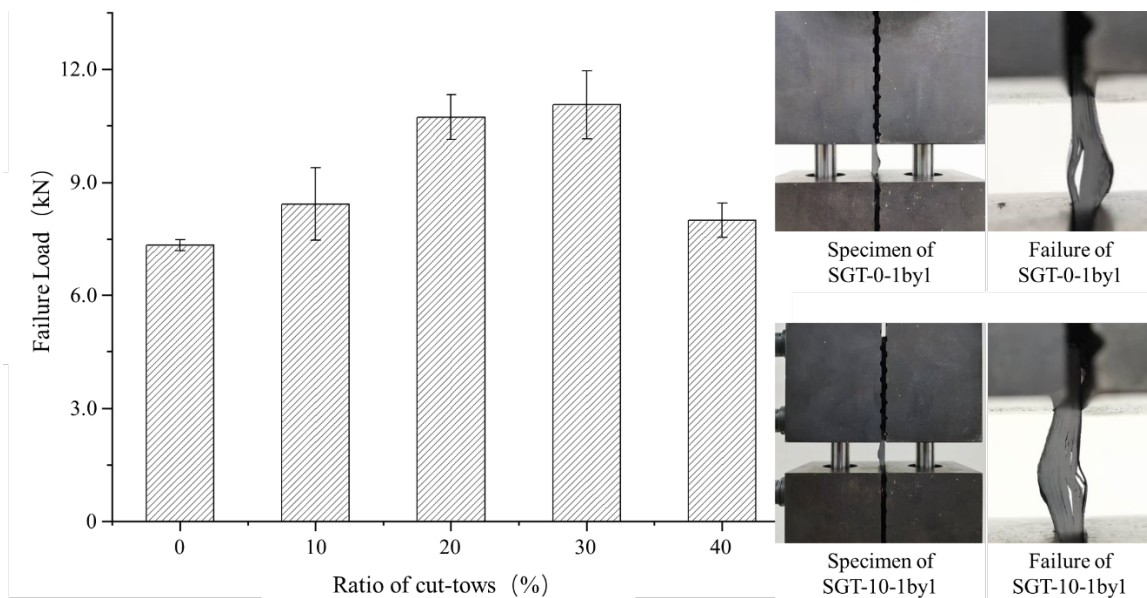


Fig. 12 Compressive failure load of thick grid stiffeners with different ratio of cut-tows.

5 CONCLUSIONS

The continuous fiber layup of the AGS results in a thicker intersection due to the overlapping of the longitudinal and transverse tows. Earlier studies have shown that a localized buckling due to tow waviness leads to potential weak point in the structure. Experimental investigation confirmed that the degree of tow waviness in the intersection reduced the compressive performance of the grids. An empirical relation had been proposed to predict the degree of tow waviness for an arbitrary grid thickness. Using the “Clamp-Cut-Restart” operation of automated fiber placement, cut-tows were introduced into the grid structure and reduce the degree to tow waviness in the specimen. The fiber placement of the tows can be achieved accurately, and no manufacturing defects were introduced in the process. A FE modelling methodology was developed and validated to analyze the deformation and damage progression in grids with varying degree of tow waviness. While no improvements was observed for cut-tows design over the SG-0-1by1, the cut-tows did not detrimentally affect the

compressive design. However, improvements over the SG-0-2by2 was observed, meaning wrapping with thick plies can benefit from this design approach. Preliminary investigations showed this design approach can be scaled to a thick grid stiffener. Further experimental validations are required to improve confidence and further optimize the design methodology.

ACKNOWLEDGEMENTS

The authors would like to acknowledge the support from National Natural Science Foundation of China (Grant No. 52005257), ARC Training Centre for Automated Manufacture of Advanced Composites (Grant No. IC160100040).

REFERENCES

- [1] Lim KH, Wei H, Guan ZD. Buckling analysis of advanced grid stiffened composite cylinders. *Advanced Materials Research: Trans Tech Publ*; 2014. p. 755-62.
- [2] Nampy SN, Smith E, Bakis C. Advanced grid-stiffened composite shells for heavy-lift helicopter blade spars. 55th AIAA/ASME/ASCE/AHS/SC Structures, Structural Dynamics, and Materials Conference 2014. p. 1062.
- [3] Huybrechts SM, Meink TE, Wegner PM, Ganley JM, Manufacturing theory for advanced grid stiffened structures, *Composites Part A: Applied Science and Manufacturing*, **33**, 2002, pp. 155-61. ([https://doi.org/10.1016/S1359-835X\(01\)00113-0](https://doi.org/10.1016/S1359-835X(01)00113-0))
- [4] Zhao C, Donough MJ, Prusty BG, Xiao J, Influences of ply waviness and discontinuity on automated fibre placement manufactured grid stiffeners, *Composite Structures*, **256**, 2021, pp. 106-13. (<https://doi.org/10.1016/j.compstruct.2020.113106>)
- [5] Wilhelmsson D, Gutkin R, Edgren F, Asp LE, An experimental study of fibre waviness and its effects on compressive properties of unidirectional NCF composites, *Composites Part A: Applied Science and Manufacturing*, **107**, 2018, pp. 665-74. (<https://doi.org/10.1016/j.compositesa.2018.02.013>)
- [6] Alves MP, Cimini Junior CA, Ha SK, Fiber waviness and its effect on the mechanical performance of fiber reinforced polymer composites: An enhanced review, *Composites Part A: Applied Science and Manufacturing*, **149**, 2021, pp. 106526. (<https://doi.org/10.1016/j.compositesa.2021.106526>)
- [7] Lamberti L, Venkataraman S, Haftka RT, Johnson TF, Preliminary design optimization of stiffened panels using approximate analysis models, *International Journal for Numerical Methods in Engineering*, **57**, 2003, pp. 1351-80. (<https://doi.org/10.1002/nme.781>)
- [8] Prusty BG. Static, Dynamic, Buckling and Failure Analyses of Composite Stiffened Shell Structures: A Finite Element Approach: Indian Institute of Technology, 2001.
- [9] Cheng G-D, Cai Y-W, Xu L, Novel implementation of homogenization method to predict effective properties of periodic materials, *Acta Mechanica Sinica*, **29**, 2013, pp. 550-6. (10.1007/s10409-013-0043-0)
- [10] Ghazlan A, Ngo T, Tan P, Xie YM, Tran P, Donough M, Inspiration from Nature's body armours – A review of biological and bioinspired composites, *Composites Part B: Engineering*, **205**, 2021, pp. 108513. (<https://doi.org/10.1016/j.compositesb.2020.108513>)
- [11] Zhao C, Donough MJ, Prusty BG, Xiao J, Zhou L, An L, Pseudo-ductile fracture in grid stiffened structure by automated fibre placement, *Composite Structures*, **308**, 2023, pp. 116694. (<https://doi.org/10.1016/j.compstruct.2023.116694>)
- [12] Rodríguez-García V, Guzman de Villoria R, Automated manufacturing of bio-inspired carbon-fibre reinforced polymers, *Composites Part B: Engineering*, **215**, 2021, pp. 108795. (<https://doi.org/10.1016/j.compositesb.2021.108795>)
- [13] Hashin Z. Fatigue Failure Criteria for Unidirectional Fiber Composites. Pennsylvania Univ Philadelphia Dept of Materials Science and Engineering; 1980.